Applied Catalysis B: Environmental 189 (2016) 110–118

Contents lists available at ScienceDirect

Applied Catalysis B: Environmental

journal homepage: www.elsevier.com/locate/apcatb

Electrochemical oxidation of ethanol on palladium-nickel nanocatalyst in alkaline media

M.D. Obradović[a], Z.M. Stančić[b], U.Č. Lačnjevac[c], V.V. Radmilović[d], A. Gavrilović-Wohlmuther[e], V.R. Radmilović[b,f], S.Lj. Gojković[b,*]

[a] Institute of Chemistry, Technology and Metallurgy, University of Belgrade, Njegoševa 12, 11000 Belgrade, Serbia
[b] Faculty of Technology and Metallurgy, University of Belgrade, Karnegijeva 4, 11120 Belgrade, Serbia
[c] Institute for Multidisciplinary Research, University of Belgrade, Kneza Višeslava 1, 11030 Belgrade, Serbia
[d] Innovation Center, Faculty of Technology and Metallurgy, University of Belgrade, Karnegijeva 4, 11120 Belgrade, Serbia
[e] Centre of Electrochemical Surface Technology, Viktor-Kaplan-Strasse 2, A-2700 Wiener Neustadt, Austria
[f] Serbian Academy of Sciences and Arts, Knez Mihailova 35, 11000 Belgrade, Serbia

ARTICLE INFO

Article history:
Received 19 October 2015
Received in revised form 11 February 2016
Accepted 16 February 2016
Available online 21 February 2016

Keywords:
Ethanol oxidation
Palladium
Nickel
Alkaline
Fuel cell

ABSTRACT

Pd-Ni/C catalyst was synthesized employing a borohydride reduction method. The high area Ni was first dispersed on the carbon support and then modified by Pd nanoparticles. Transmission electron microscopy confirmed relatively even distribution of Ni across the carbon support with discrete palladium particles of about 3.3 nm mean diameter on it. Cyclic voltammetry confirmed the presence of Ni on the catalyst surface. The activity of the Pd-Ni/C catalysts for ethanol oxidation reaction (EOR) in alkaline solution was tested under the potentiodynamic and potentiostatic conditions and the results were compared to those obtained on the Pd/C catalyst. It was found that Pd-Ni/C is more active for the EOR compared to Pd/C by a factor up to 3, depending on the type of experiments and whether specific activity or mass activity are considered. During the potentiodynamic stability test an interesting phenomenon of activation of Pd-Ni/C catalyst was observed. It was found that maximum activity is attained after fifty cycles with the positive potential limit of 1.2 V, regardless of whether they were performed in the electrolyte with or without ethanol. It was postulated that potential cycling of the Pd-Ni surface causes reorganization of the catalyst surface bringing Pd and Ni sites to a more suitable arrangement for the efficient ethanol oxidation.

1. Introduction

Direct alcohol fuel cells (DAFCs) are recognized as promising power sources for portable electronic devices and electric vehicles [1]. Although DAFC driven by methanol oxidation in acidic media is the most common and commercially available [2], ethanol as a fuel attracts increasing attention because it can be produced from fermentation of biomass [3], it is a low-toxic liquid and its crossover through the polymer membrane is lower than that of methanol [4]. In acidic media ethanol can be oxidized only on Pt-based catalysts, but the reaction is rather sluggish for efficient operation of direct ethanol fuel cells (DEFC) [1]. However, in alkaline media ethanol oxidation reaction (EOR) is faster [5,6], and interestingly, Pd shows greater activity for the EOR in this environment than Pt [7–10]. This shows opportunity of the development of DEFC since Pd is less expensive than Pt [11] and the development of anion exchange membranes [12] is in progress. In addition, numerous metals are stable in alkaline media and can be used for designing bi- and tri-metal catalysts [9,10,13].

Higher activity of Pd compared to that of Pt for the EOR is attributed to its more oxophilic nature [6] that facilitates oxidative desorption of intermediate species. The same rationale is behind introducing Ni in electrocatalysts for the EOR. Although Ni itself is not active for the EOR at the potentials relevant for DEFC operation [14], various Pd-Ni electrocatalysts exhibited enhanced activity and greater tolerance to catalyst poisoning compared to pure Pd [15–24].

Shen and Xu [13] were the first to report that the EOR on Pd–NiO/C commences at 150 mV lower potential than on Pd/C and even 250 mV lower potential than on Pt/C catalysts. Higher activity and decreased poisoning of Pd–NiO/C compared to the Pt–NiO/C electrocatalyst for the EOR was reported by Hu et al. [15]. Neg-

* Corresponding author.
E-mail address: sgojkovic@tmf.bg.ac.rs (S.Lj. Gojković).

http://dx.doi.org/10.1016/j.apcatb.2016.02.039
0926-3373/

atively shifted onset potential and doubled peak current density in potentiodynamic conditions for core-shell Ni-Pd/C compared to Pd/C was found by Zhang et al. [20]. High activity and excellent stability in potential cycling conditions were found for Pd supported on Ni foam in the study by Wang et al. [16]. Pd-Ni/C catalysts with various ratios of Pd and Ni were also investigated [17,18,22,24]. Irrelevant of the method of preparation and the structure, all studies show that the catalysts containing between 50 and 60 at.% of Ni are the most active and stable. In the work by Dutta and Datta [24] clear correlation between the alloying degree and the activity was established as the more alloyed Pd–Ni particles were more active. The same influence of the metal alloying was found by Ahmed and Jeon [22]. In the Pd-Ni/C catalysts investigated by Shen et al. [17] and Zhang et al. [18] Pd and Ni did not alloy well, but their performance was still improved compared to Pd/C. These results suggest that the capacity of Ni to generate OH_{ads} species at lower potential and facilitate the oxidative desorption of intermediates in the EOR is crucial for the enhanced activity of Pd, although the ligand and strain effects also contribute. The insertion of substitutional Ni atoms into the Pd crystal lattice causes a contraction of the Pd lattice because of a smaller Ni radius (135 pm for Ni and 140 pm for Pd). This causes a downshift of the Pd d-band center and consequently leads to weaker bonding with adsorbates such as poisoning intermediates in the EOR. In addition, since Pd has a higher ionization energy than Ni (8.34 eV compared to 7.63 eV, respectively), Ni atoms become positively charged, which facilitates the formation of oxides on Ni [24].

The mechanism of the EOR on polycrystalline Pd was investigated by Fang et al. [25] using in situ FTIR spectroscopy. In the solutions with pH < 13.3 they detected acetate ions and CO_2, but in more alkaline solutions the CO_2 band was absent. Interestingly enough, no trace of CO was detected even at pH 12. It was concluded that the cleavage of the C—C bond occurs only at lower pH values where a non-poisoning reaction path is likely to take place. Zhou et al. [26] also found that acetate is the main product and that CO_2 and carbonate ions appear only at potentials too high for DEFC application. However, they detected a weak signal of CO_{ads} suggesting that complete oxidation of ethanol might be achieved through an indirect pathway. In FTIR spectra for Pd black only the bands of acetate are observed. Liang et al. [27] investigated the EOR on Pd in a wide range of ethanol and hydroxide concentrations. Based on the polarization measurements of ethanol, acetaldehyde and potassium acetate oxidation, the authors suggested that the dissociative adsorption of ethanol proceeds rather quickly and that the rate-determining step is the removal of the adsorbed CH_3CO particles by the adsorbed hydroxyl on the Pd electrode. In the study of the EOR on Pd/C and Pd-Ni/C, Dutta and Datta [24] found acetate and carbonate ions as the final reaction products by using ion exchange chromatography. For the Pd/C catalyst, the acetate ions were predominant, while on the best performing $Pd_{37}Ni_{63}$/C catalyst, carbonate ions slightly outbalanced acetate ions. DFT calculation by Cui et al. [28] confirmed that the dehydrogenation of ethanol is possible only in alkaline media where adsorbed OH species are abundant. The formation of acetaldehyde was predicted as the first step during the EOR, and it could be further oxidized. Based on these results, the following mechanism of the EOR on Pd in alkaline media has been proposed [27]:

$$Pd + OH^- \rightleftarrows PdOH_{ads} + e^- \quad (1)$$

$$Pd + CH_3CH_2OH \rightleftarrows Pd\text{–}(CH_3CH_2OH)_{ads} \quad (2)$$

$$Pd\text{–}(CH_3CH_2OH)_{ads} + 3OH^- \rightarrow Pd\text{–}(CH_3CO)_{ads} + 3H_2O + 3e^- \quad (3)$$

$$Pd\text{–}(CH_3CO)_{ads} + PdOH_{ads} \xrightarrow{rds} Pd\text{–}CH_3COOH + Pd \quad (4)$$

$$Pd\text{–}CH_3COOH + OH^- \rightarrow Pd + CH_3COO^- + H_2O \quad (5)$$

For potentials below 0.6 V (RHE) it is suggested that the first stage in Pd oxidation, given by Eq. (1), is the rate determining step [29]. It is believed that Ni promotes the EOR on Pd by supplying adsorbed OH species at lower potentials, which influences the onset of the EOR. In addition, in the whole potential region, the OH species from the Ni sites facilitate the stripping of reaction intermediates, which recovers the Pd sites and thereby accelerates further oxidation of ethanol molecules [23].

In order to employ the beneficial effects of Ni on EOR activity of Pd-Ni catalysts, in this work we synthesized high surface area Ni on carbon support and modified it with Pd nanoparticles. Such a structure of the catalyst is different compared to conventional core/shell, alloyed or non-alloyed Pd-Ni nanoparticles. In this way Pd nanoparticles when immersed in an alkaline medium are surrounded by an abundance of OH groups attached to the Ni atoms. The Pd-Ni/C catalyst was characterized and its activity for the EOR in alkaline electrolytes was evaluated. The results were compared to those obtained on a Pd/C catalyst. The phenomenon of the activation of the Pd-Ni/C catalyst during the potential cycling was explored. It was found that the specific activity of Pd for the EOR can be doubled by the presence of Ni.

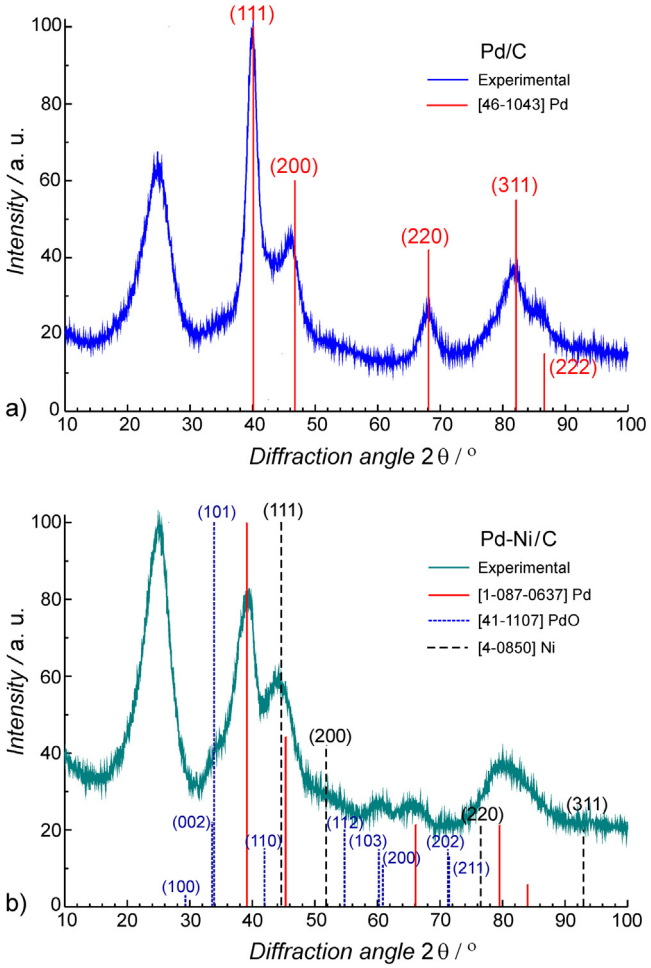

Fig. 1. XRD patterns of prepared catalysts: (a) Pd/C and (b) Pd-Ni/C. The lines represent 2θ positions and corresponding intensities of the diffraction peaks for Pd, PdO and Ni crystal structures according to the ICDD-PDF cards.

2. Experimental

2.1. Preparation of the catalyst

The Pd-Ni/C catalyst was prepared by a two-step procedure in which a non-noble metal is chemically deposited on the carbon support and then covered by a noble metal [30,31]. Briefly, high area carbon (Vulcan® XC-72R, surface area 248 $m^2 g^{-1}$) was dispersed in high purity water (Millipore, 18 MΩ cm resistivity) in an ultrasonic bath while the suspension was purged with nitrogen. At that point 0.02 M $Ni(HCOO)_2$ and 0.5 M $Na_3C_6H_5O_7$ solutions at a ratio of 1:5 were added into the suspension. After 60 min of agitation, the reduction of Ni ions was initiated by adding 0.1 M $NaBH_4$. The molar ratio of Ni and $NaBH_4$ was 1:2. After 5 min the solution of 5×10^{-3} M $PdCl_2$ was added into the reaction mixture (atomic ratio of Ni to Pd was 3:1) and left under the ultrasonic agitation for over 1 h. The suspension was then filtered and the precipitate was washed by a 0.02 M NH_3 solution. The remaining solid material was dried under nitrogen atmosphere at 80 °C for 6 h.

For a comparison of voltammetric features and electrocatalytic activity, a Pd/C sample was prepared. Similarly to the procedure for Pd-Ni/C synthesis, powder of Vulcan® XC-72R carbon was dispersed in water in an ultrasonic bath and $PdCl_2$ aqueous solution was added into suspension under continuous stirring. After adjusting the suspension pH to 10 by adding 0.1 M NaOH solution, the metal salt was slowly reduced in the presence of excess 0.5 M $NaBH_4$ solution under continuous stirring at 40 °C. The suspension was then filtered and the precipitate was washed with a 0.02 M NH_3 solution. The remaining solid material was dried under the nitrogen atmosphere at 80 °C for 6 h.

Voltammetric and electrocatalytic characteristics of Ni were investigated on a bulk Ni electrode in the form of a disk.

2.2. Physico-chemical characterization

The total metal loadings of the Pd-Ni/C and Pd/C catalysts were determined by thermogravimetric analysis (TGA) using a SDT Q600 TGA/DSC instrument (TA Instruments). Several milligrams of the sample were heated to 1000 °C at the rate of 20 °C min^{-1}. The temperature was first increased in the nitrogen atmosphere from room temperature to 500 °C. After holding at 500 °C for 10 min, the gas was switched from nitrogen to air and the sample was further heated to 1000 °C [18]. The gas flow rate was 100 cm^3 min^{-1}.

The average ratio of Pd and Ni in the Pd-Ni/C catalyst was determined by energy-dispersive X-ray spectroscopy (EDS) using a scanning electron microscope Tescan VEGA TS 5130MM coupled with an EDS system INCAPentaFET-x3, Oxford Instruments.

Transmission electron microscopy (TEM) was employed to analyze the morphology, particle size distribution and chemical composition of the catalysts. The samples were sonicated in ethanol and drop cast on a Cu grid (300 mesh) covered by a lacey carbon film and dried in air. High angle annular dark field Scanning transmission electron microscopy (HAADF, STEM) and high resolution phase contrast transmission electron microscopy (HRTEM) were performed on the FEI TITAN^3 Themis 60–300 double aberration corrected microscope equipped with the Super-X Energy Dispersive Spectrometry (SuperX EDS) system controlled with Bruker Esprit software. The maps were obtained using Pd and Ni L lines. Crystallographic information from individual particles was obtained by numerical Fourier filtering (FFT, Fast Fourier Transformation) of HRTEM micrographs. These experiments were performed at the Center for Nanoanalysis and Electron Microscopy (CENEM), University Erlangen-Nürnberg, Erlangen, Germany.

X-ray diffraction (XRD) experiments were performed on an X-Pert powder diffractometer (PANalytical) using Cu Kα radiation in Bragg–Brentano geometry at 45 kV and 40 mA. This diffractometer is equipped with a secondary graphite monochromator. The measurements were conducted in step-scan mode in 0.05° (2θ) intervals with a measuring time of 25 s/step. In order to minimize background, Si (511) single crystal was used as a sample holder. The TOPAS V3 general profile and structure analysis software for powder diffraction data was used for the Rietveld refinement procedure [32].

2.3. Electrochemical measurements

For the electrochemical characterization, the Pd-Ni/C and Pd/C catalysts were applied on a glassy carbon (GC) substrate in the form of a thin–film. The GC electrode (Tacussel rotating disk electrode, 5 mm in diameter) was polished with Al_2O_3 slurry and washed ultrasonically with water before use. The ink was made by mixing 2.0 mg of the Pd-Ni/C or Pd/C powders with 1 cm^3 of high purity water and 50 μL of the Nafion® solution (5 wt.%, 1100 E.W., Aldrich) followed by 1 h of agitation in an ultrasonic bath. For each experiment a new portion of 10 μL of the suspension was placed onto the GC electrode and left to dry overnight.

The Ni electrode was polished with Al_2O_3 slurry and washed ultrasonically with water before use.

Voltammetric characterization of the electrocatalysts was performed in a 0.1 M NaOH solution and in some cases in 0.1 M H_2SO_4. Electrochemical oxidation of ethanol was examined in the alkaline supporting electrolyte containing 0.5 M ethanol.

After immersing the Pd-Ni/C or Pd/C electrode in the supporting electrolyte, the electrode potential was cycled between 0.06 V and 1.2 V over 10 cycles at the scan rate of 100 mV s^{-1}, then the scan rate was adjusted to 50 mV s^{-1} and the second voltammogram was used for the determination of the electrochemically active surface area (EASA). Upon such a preconditioning of the electrode surface, in a positive-going scan the electrode potential was held at 0.35 V and ethanol was added into the electrolyte. In the experiments in which EOR was examined under the potentiodynamic conditions, after 2 min the potential cycling between 0.35 V and 1.2 V was continued. For studying EOR under the potentiostatic conditions, instead of continuation of the potential cycling, the potential was stepped from 0.35 V to 0.5 V or 0.7 V.

Besides cyclic voltammograms recorded in 0.1 M NaOH, the EASA of Pd/C was also determined by CO_{ads} stripping in an acid solution. In this experiment the potential was cycled between 0.06 V and 1.2 V and after 10 cycles in a positive-going scan the electrode potential was held at 0.2 V for 30 min while bubbling pure CO through the electrolyte. After purging the electrolyte by N_2 for 30 min to eliminate dissolved CO, CO_{ads} was oxidized in an anodic scan at 20 mV s^{-1}. Two subsequent voltammograms were also recorded to verify the completeness of the CO_{ads} oxidation.

All the experiments were performed in a three-compartment electrochemical glass cell with a Pt wire (99.998% purity, Alfa Aesar) as the counter electrode and a saturated calomel electrode (SCE) as the reference electrode. The potentials reported in the paper are expressed on the scale of the reversible hydrogen electrode (RHE). The electrolytes were prepared with high purity water and the chemicals provided by Merck. The experiments were conducted at 298 ± 0.5 K. A Pine RDE4 potentiostat and Philips PM 8143 X–Y recorder were employed.

3. Results and discussion

3.1. Average elemental composition of the catalyst

Total metal loadings of the Pd-Ni/C and Pd/C catalysts, determined by TGA measurements, were found to be 11.3 mass% and 8.0 mass%, respectively. The ratio of Pd and Ni in the Pd-Ni/C catalyst

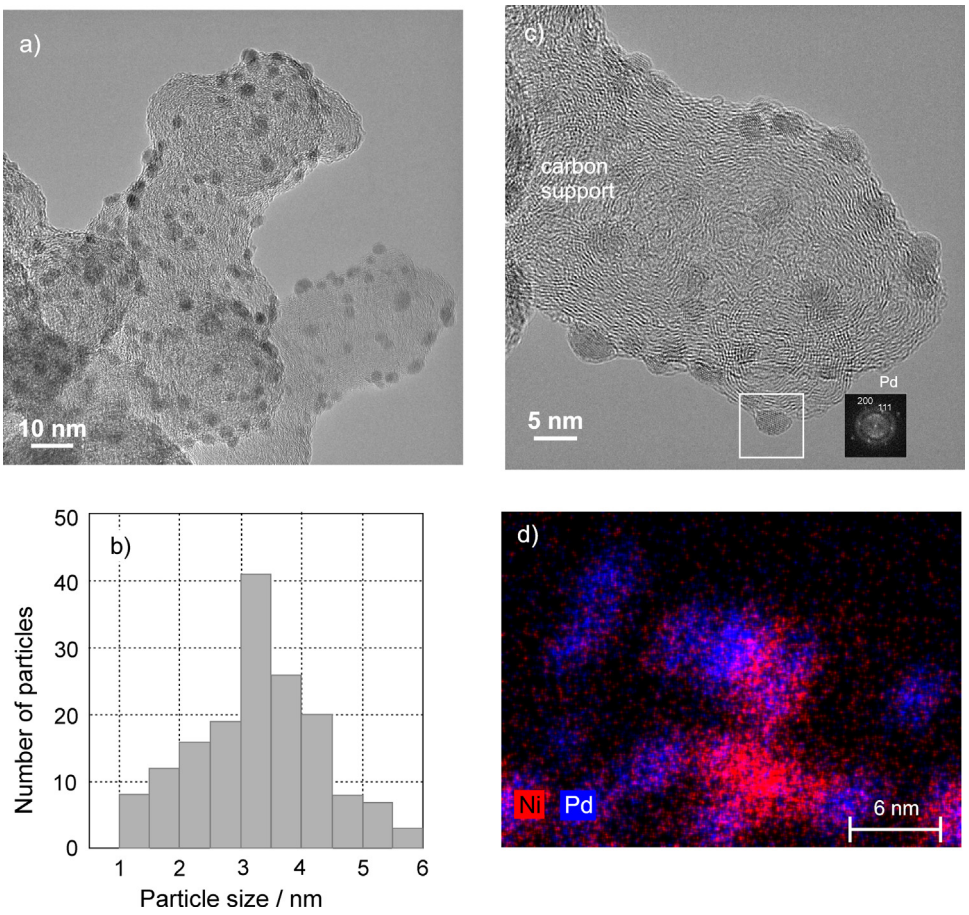

Fig. 2. STEM characterization of the Pd-Ni/C catalyst: (a) low magnification micrograph, (b) histogram of the particle size distribution, (c) Pd particle with FFT close to 110 zone axis and (d) EDS elemental mapping showing Ni and Pd distribution on carbon support.

was determined by EDS. The analysis was applied at five different places with surface area ranging from about 150 μm × 150 μm to about 600 μm × 600 μm. The average Pd to Ni atomic ratio of 0.40:0.60 was calculated. Taking into account the total metal loading, the Pd-Ni/C catalyst contained 6.2 mass% of Pd.

3.2. XRD characterization

The XRD pattern of the Pd/C catalyst is presented in Fig. 1a. The first broad peak at the 2θ value of about 25° is attributed to the Vulcan® XC-72R carbon support. The other peaks are consistent with a face centered cubic (FCC) crystal structure of Pd. The Rietveld refinement procedure revealed Pd lattice parameter value of 0.3907 nm. Using the Scherrer equation [33] the crystallite size of 3 ± 1 nm was determined. The XRD pattern of the Pd-Ni/C powder, displayed in Fig. 1b, indicates a multiphase structure of this catalyst. In addition to the peaks of Pd, the peaks of PdO are present, while the peaks of metallic Ni can vaguely be observed. The Rietveld analysis showed a slightly larger Pd lattice parameter (0.4002 nm) that suggests that Pd and Ni are not alloyed in the catalyst, because alloying Pd with Ni would decrease the lattice parameter due to the smaller size of Ni atoms. The crystallite size of Pd in the Pd-Ni/C catalyst was estimated to be 2 ± 1 nm.

3.3. TEM characterization

A low magnification STEM image of the Pd-Ni/C catalyst given in Fig. 2a shows well dispersed metallic particles on carbon support. Most of the larger particles are not single grains but agglomerates of smaller particles. Taking this into account, the particle size distribution with the mean particle size diameter of 3.3 nm was determined (Fig. 2b). The surface-averaged diameter, $\bar{d}_s$, was calculated as well. By applying the equation:

$$\bar{d}_s = \frac{\sum_{i=1}^{n} n_i d_i^3}{\sum_{i=1}^{n} n_i d_i^2} \quad (6)$$

where n_i stands for the number of particles having a diameter d_i, the $\bar{d}_s$ value was found to be 3.9 nm.

A closer inspection of the particles using high resolution TEM (HRTEM), shown in Fig. 2c, indicates that some of them are pure Pd, while others consist of both Pd and Ni. However, the origin of the Ni signal could also be coming from the area below or above particles containing Pd. Otherwise it would be very difficult to understand why some particles would contain Ni and Pd while others only Pd.

In order to gain better insight into the distribution of the elements in the sample, numerous EDS maps have been collected. Most of them show that Ni is distributed relatively evenly across the carbon support, while palladium forms discrete particles (Fig. 2d). This means that Ni served as a template for Pd precipitation, which permitted close contact between the metals necessary for their synergistic catalytic activity.

STEM imaging of Pd/C catalyst showed well dispersed Pd nanoparticles on the high area carbon support (Fig. S1). The mean

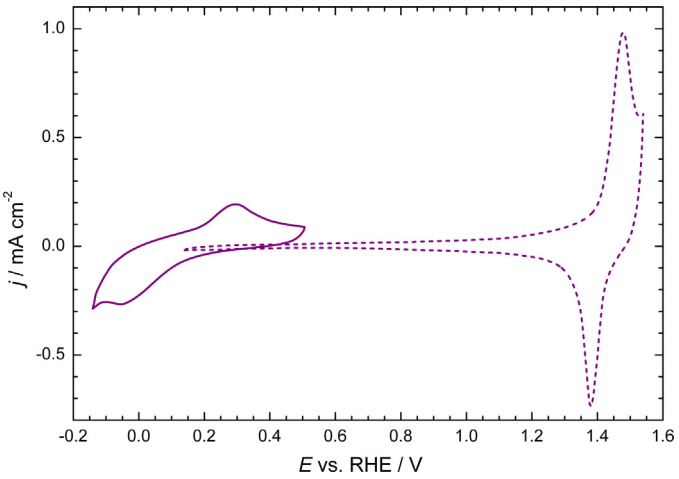

Fig. 3. Cyclic voltammograms of a Ni electrode within different potential windows recorded in 0.1 M NaOH with the scan rate of 100 mV s^{-1}.

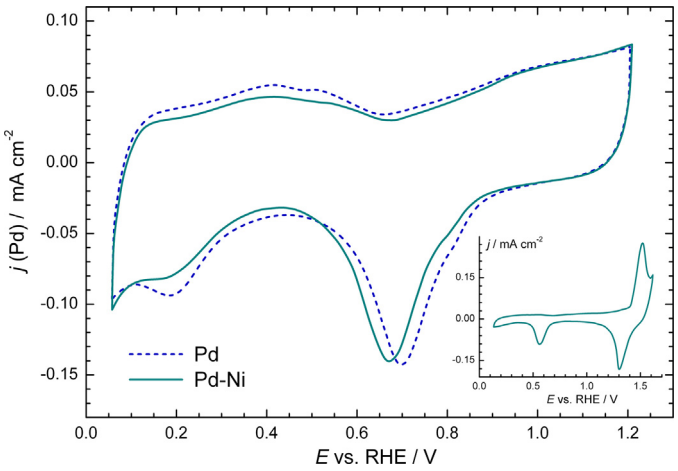

Fig. 4. Cyclic voltammograms of Pd/C and Pd-Ni/C catalysts recorded in 0.1 M NaOH with the scan rate of 50 mV s^{-1}. Inset: Cyclic voltammogram of Pd-Ni/C with the extended positive potential limit.

particle size diameter of 3.7 nm and surface-averaged diameter of 4.1 nm were determined.

3.4. Electrochemical characterization of the catalysts

Before performing a voltammetric study of the bimetallic Pd-Ni/C catalyst, the cyclic voltammograms of pure Ni and pure Pd surfaces were explored. Fig. 3 shows cyclic voltammograms of a Ni electrode with the extending positive potential limit. In the first cycle with the positive limit of 0.5 V one can observe a pair of peaks at 0.3 V and −0.05 V, which can be ascribed to the transition between Ni and α-$Ni(OH)_2$ [34]. It is believed that a monolayer of α-$Ni(OH)_2$ is formed, so the charge under the peak can be used for the estimation of the EASA of Ni [35]. When the positive potential limit is extended to 1.2 V, the peaks disappear (not shown) because of the formation of β-$Ni(OH)_2$ that cannot be electrochemically reduced. At more positive potentials a pair of sharp peaks at 1.48 V and 1.35 V develops, which is attributed to further oxidation of Ni(II) species to a form of NiOOH and its reduction [34]. The anodic peak partially overlaps with oxygen evolution, so the charge under the cathodic peak corresponds to the amount of the NiOOH formed. Since this charge exceeds the one under the anodic peak at 0.3 V, even though the formation of NiOOH is a one-electron process in contrast to a two-electron formation of α-$Ni(OH)_2$, it is obvious that more than a monolayer of NiOOH is present on the electrode surface.

In Fig. 4 cyclic voltammograms of Pd/C and Pd-Ni/C recorded in 0.1 M NaOH are overlaid. As can be seen, their features are close to each other. The hydrogen adsorption/desorption peaks (0.16 V/0.43 V) are not well distinguished as they are in acid media [36]. Moreover, hydrogen desorption is overlapping with the adsorption of OH^- ions, featured in anodic peaks positioned at about 0.60 V. Pd(II)-oxide starts to grow at about 0.68 V and attains a complete monolayer at potentials around 1.2 V [37,38], after which the formation of Pd(IV) oxide begins. Reduction of Pd(II)-oxide on both catalysts produces a well-defined peak, but at different potentials. On Pd/C the peak maximum is at 0.70 V while on Pd-Ni/C it is attained at a value about 0.04 V latter, which indicates a stronger adsorption of oxide species on the Pd-Ni surface than on pure Pd. It should be noted that stronger adsorption of oxide species on Pd on Pd-Ni surface might be due to a smaller Pd particle size comparing to Pd in Pd/C catalyst, but since the difference in the size is small, it is more likely related to the contact of Pd with Ni. The voltammogram of Pd-Ni/C with the high anodic potential limit, presented in the inset in Fig. 4, confirms the presence of Ni on the surface of the catalyst.

Estimation of the EASA of Pd in the Pd/C catalyst was based on the charge of CO_{ads} stripping in an acid solution and the charge of Pd(II)-oxide reduction in an alkaline solution. Firstly, a CO_{ads} stripping experiment was carried out in an acid solution (Fig. S2); the charge under the peak was determined and the EASA of Pd was calculated assuming that 420 μC cm^{-2} corresponds to the monolayer of CO_{ads} [39]. At this point, the electrode was transferred into a cell with an alkaline solution, the voltammogram was recorded and the charge for Pd(II)-oxide reduction was determined. Using this value and the EASA calculated in the previous CO_{ads} stripping experiment, it was calculated that the same value of 420 μC cm^{-2} is consumed for the of Pd(II)-oxide reduction. Thus, we suppose that complete monolayer of Pd(II)-oxide is attained with the positive potential limit of 1.2 V, which corresponds to the finding of Bolzán [37] and Grdeń [38]. The value of 420 μC cm^{-2} is close to 424 μC cm^{-2} and 405 μC cm^{-2} that were used for EASA determination in the works of Rand and Woods [40] and Wang et al. [41], respectively. Therefore, the EASA of Pd in any particular experiment, either on Pd/C or Pd-Ni/C catalyst, was determined by integration of the cathodic peak for Pd(II)-oxide reduction and this value was used for calculating of the current density of ethanol oxidation.

Surface composition of the Pd-Ni/C catalyst was estimated by calculation of real surface area of Ni. From the ratio of the charges beneath the peaks at 1.38 V and 0.3 V for pure Ni (Fig. 3) and the charge under the cathodic peak at 1.30 V on the voltammogram of Pd-Ni/C (Inset in Fig. 4), the charge for the formation of α-$Ni(OH)_2$ on Pd-Ni/C, which is not visible on that voltammogram, was calculated. Using the value of 514 μC cm^{-2} as the charge for a monolayer of α-$Ni(OH)_2$ [35], the EASA of Ni was estimated. From several independent experiments the average surface ratio of Pd to Ni in the Pd-Ni/C catalyst was determined at 0.22:0.78. A higher concentration of Ni sites at the surface of Pd-Ni/C with respect to the bulk Ni content determined by EDS analysis (Pd:Ni = 0.40:0.60) suggests a finer dispersion of precipitated Ni particles compared to Pd. This conclusion is in accordance with the EDS mapping analysis (Fig. 2d).

3.5. Evaluation of electrocatalytic activity for the EOR

The activity of the Pd-Ni/C and Pd/C catalysts for the EOR was initially tested under potentiodynamic conditions. The electrodes were subjected to 250 potential cycles between 0.35 V and 1.2 V in an electrolyte containing ethanol. Fig. 5a displays the second anodic scans after the addition of ethanol in the electrolyte, which are chosen to represent the initial activity under the potentiodynamic conditions. As can be seen, the onset potentials on those two cata-

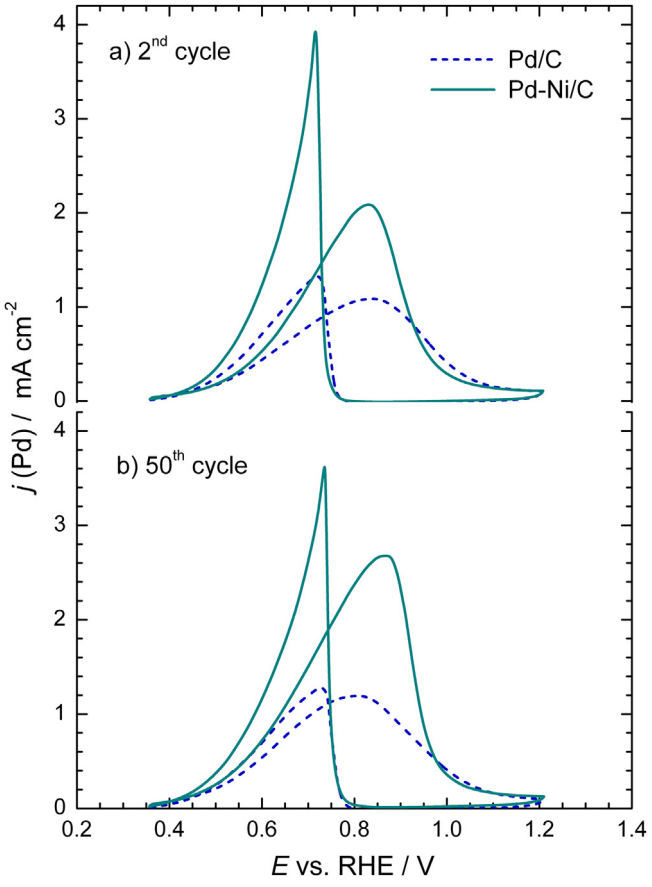

Fig. 5. Potentiodynamic polarization curves for the EOR on Pd/C and Pd-Ni/C catalysts recorded in 0.1 M NaOH containing 0.5 M C_2H_5OH at the scan rate of 50 mV s^{-1}: (a) 2nd cycle and (b) 50th cycle.

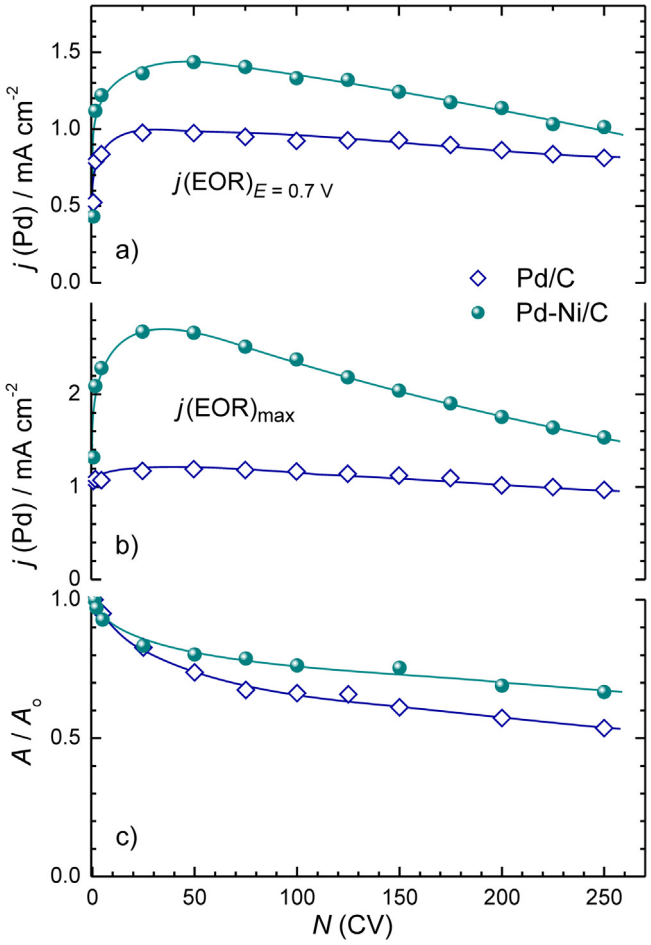

Fig. 6. The current densities for the EOR on Pd/C and Pd-Ni/C catalysts in 0.1 M NaOH containing 0.5 M C_2H_5OH as a function of the cycle number: (a) taken at 0.7 V and (b) maximum current densities. c) EASA of Pd in Pd/C and Pd-Ni/C catalysts normalized with respect to the initial EASA. Potential cycling performed at the rate of 50 mV s^{-1}.

lysts are similar, but from about 0.5 V, the Pd-Ni/C catalyst exceeds the Pd/C in EOR activity. At the current maximum attained at 0.83 V the current density on Pd-Ni/C is higher than on Pd/C by a factor of 1.9. It should be recalled that the current densities are expressed per EASA of Pd for both catalysts. A decrease in the EOR current at higher potentials caused by Pd(II)-oxide growth is observed, which is typical for oxidation of organic molecules on noble metals like Pt and Pd. This is because organic molecules can be adsorbed on bare but not on the oxidized Pd or Pt surface. In the reverse scan the EOR on Pd-Ni/C starts slightly later than on Pd/C, which is in agreement with the delayed Pd(II)-oxide reduction in the presence of Ni (cyclic voltammograms in Fig. 4). Fig. 5b presents the potentiodynamic curves in the 50th scan. The curves for Pd-Ni/C and Pd/C are qualitatively the same as those at the beginning of potential cycling, while the maximum current density on Pd-Ni/C is higher by a factor of 2.2. The activity of pure Ni for the EOR was also tested. It was found that Ni can oxidize ethanol but only at the potentials where NiOOH develops. In the potential range where Pd-Ni/C was investigated Ni is completely inactive for the EOR.

The results of the activity test for up to 250 cycles are presented in Fig. 6. The currents at the potential of 0.7 V taken from the anodic scans were corrected for the background currents and normalized to the EASA determined at the beginning of the experiment. The resulting current densities are plotted as a function of the cycle number (Fig. 6a). The reproducibility of this type of experiment was checked in the six independent measurements and all the data sets showed the same behavior (Fig. S3). Both Pd-Ni/C and Pd/C exhibit a large increase in activity between the first and the second cycle. In the case of Pd/C the activity remains almost constant over the next 250 cycles. However, the activity of Pd-Ni/C increases up to the 50th cycle after which it starts to decline. At the end of the test Pd-Ni/C exhibited higher current density than Pd/C by a factor of 1.3. The same trend in the activities of Pd-Ni/C and Pd/C during the cycling is observed when the maximum current densities are compared (Fig. 6b).

After the 250th potential cycle the electrode was transferred into a cell filled with the supporting electrolyte and the cyclic voltammogram was recorded. By calculating the charge beneath the peak for the reduction of Pd(II) oxide the EASA of Pd was determined. For the Pd-Ni/C catalyst a decrease of 45% with respect to the initial EASA was found, while in the case of Pd/C the EASA decrease was 35%. It should be mentioned that the peak potentials for the Pd(II) oxide reduction were the same as on the voltammograms prior to EOR, as shown in Fig. S4.

The potential cycling of Pd-Ni/C and Pd/C catalysts was also performed in the electrolyte without ethanol in the same potential limits as in the previous experiments in order to follow the gradual changes in the EASA of Pd. Fig. 6c presents the EASA over 250 cycles normalized per its initial value. The results show that a decrease in EASA of Pd in Pd-Ni/C and Pd/C at the end of the test was 30% and 45%, respectively.

Although the decrease in EASA of Pd after 250 potential cycles are not the same in the supporting electrolyte and in the ethanol containing electrolyte, the values for both Pd-Ni/C and Pd/C are roughly between 30% and 45%. However, EOR current densities at 0.7 V in the 2nd and 250th cycles are almost the same on both Pd-Ni/C and Pd/C catalysts (Fig. 5a). Besides, the maximum in the EOR

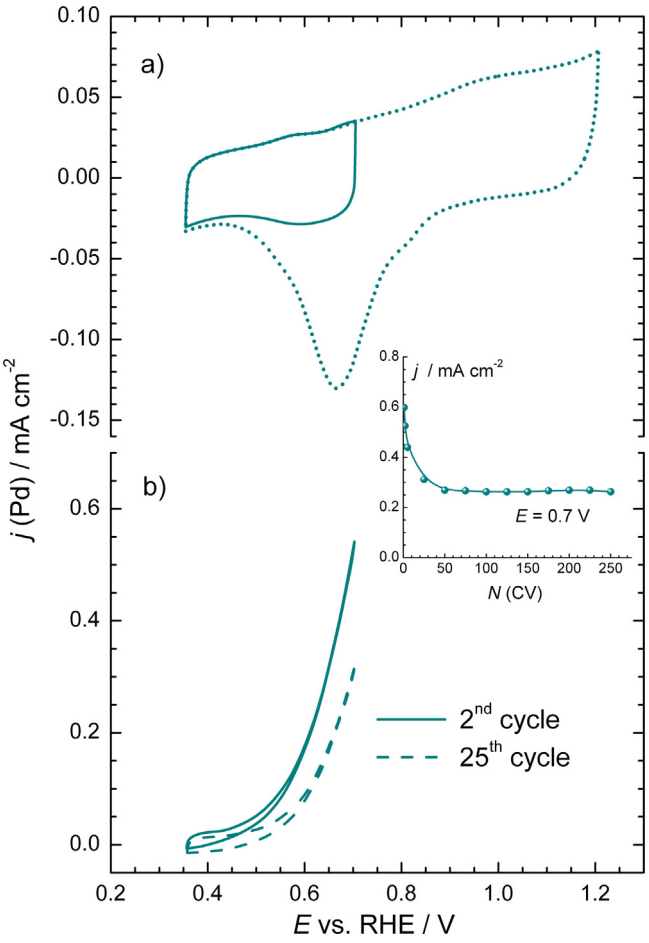

Fig. 7. (a) Cyclic voltammograms recorded on the Pd-Ni/C catalyst in 0.1 M NaOH at different positive potential limits; (b) Potentiodynamic polarization curves for the EOR on Pd-Ni/C catalysts recorded in 0.1 M NaOH containing 0.5 M C_2H_5OH at the scan rate of 50 mV s^{-1}. Inset: the current densities for the EOR taken at 0.7 V as a function of the cycle number.

activity of Pd-Ni/C cannot be correlated with the changes in EASA of Pd in this catalyst, since Fig. 5c shows monotonous decline in EASA. All these results indicate that changes in EOR activity of Pd-Ni/C and Pd/C catalysts are not simply consequence of changes in EASA, but more likely in the quality of the Pd(II) oxide.

The increase in EOR current density on Pd-Ni/C at the beginning of the potential cycling stability test followed by a slow decline has already been reported in literature [22]. It is not quite clear what causes such a behavior. In order to gain further insight into this phenomenon, some additional experiments were performed.

In the first experiment, after recording the voltammogram for EASA determination, the positive potential limit was set to 0.7 V (cyclic voltammogram in Fig. 7a) and in the second cycle ethanol was added into the electrolyte. Potential cycling was continued and the activity for the EOR was followed for over 250 cycles. The potentiodynamic curves recorded in the second and 25th cycle presented in Fig. 7b show that the hysteresis between the forward and the backward scans is negligible, but instead of an increase in activity, a substantial decrease is observed. The current densities at the constant potential of 0.7 V over the entire test are given in the inset of Fig. 7. It can be seen that the activity continues to drop until the 50th cycle after which it remains constant.

In another experiment, the Pd-Ni/C catalyst was subjected to fifty potential cycles with the positive potential limit of 1.2 V in the supporting electrolyte, after which ethanol was added into the cell. A sudden rise in the EOR current density between the first and the second cycle was observed, but with no further increase in the activity. The current density at 0.7 V in the second cycle was around 1.5 mA cm^{-2}, which is similar to the maximum current for the same catalyst in Fig. 6a. Over the next 250 cycles the current density gradually decreased.

It can be concluded that potential cycling of Pd-Ni/C catalyst up to a high positive limit like 1.2 V is required for its high activity for the EOR. Regardless of whether the initial potential cycling was made in an electrolyte with or without ethanol, the maximum current density of about 1.5 mA cm^{-2} (at the potential of 0.7 V) is achieved after fifty cycles. During further potential cycling the activity gradually decreases.

Before discussing the increase in EOR activity of Pd-Ni/C caused by the potential cycling, the reason for the enhanced activity of Pd-Ni/C catalyst comparing to Pd/C should be clarified. Inactivity of pure Ni for the EOR implies a synergism between Pd and Ni in the catalysis of this reaction. Being a highly oxophilic metal, Ni can donate oxygen containing species to the ethanol residues adsorbed on Pd atoms thus facilitating their oxidative removal from the surface (Eq. (4) in the proposed mechanism of the EOR). This is a well-established bi-functional mechanism in electrocatalysis [42]. In addition, adsorption of water and/or OH^- ions participating in Pd oxidation was found to be more significant on Pd-Ni alloys than on pure Ni [43]. Both effects require a close contact of two metals. During the potential cycling with the positive potential limit of 1.2 V a repetitive formation of Pd(II)-oxide and its reduction occur. This may cause roughening of the Pd surface, but this effect was not observed during the potential cycling of Pd/C. On the contrary, the EASA of Pd decreased, which was assumed to be a consequence of incomplete oxide reduction. It is possible that Ni oxide becomes electrocatalytically active due to potential cycling. However, no changes in otherwise featureless cycling voltammogram of Ni (Fig. 3) were detected in the experiment in the supporting electrolyte, so activation of Ni can be ruled out. A tentative explanation could be that the potential cycling of Pd-Ni surface causes reorganization of the catalyst surface bringing Pd and Ni sites to a more suitable arrangement for the efficient ethanol oxidation. It turned out to be that about fifty cycles up to 1.2 V, regardless of whether they are made in an electrolyte with or without ethanol, provide the optimum surface structure of the catalyst that yields the highest activity for the EOR.

The potentiostatic test of EOR activity was performed during 25 min at the potentials of 0.5 V and 0.7 V. At 0.5 V the EOR current densities decays steeply within few minutes and then reach almost constant but low value. The difference between the curves for Pd-Ni/C and Pd/C are minor (Fig. S4), which is in accordance with the potentiodynamic curves in Fig. 5 showing that the current densities at Pd-Ni/C and at Pd/C at 0.5 V are the same in the second cycle (Fig. 5a) and only negligibly higher on Pd-Ni/C in 50th cycle. The second potentiostatic test was carried out at a potential of 0.7 V at which approximately a half of the maximum current on the potentiodynamic curve is reached. As on 0.5 V, a rapid decay in the EOR activity for both Pd-Ni/C and Pd/C catalysts within the first minute of the test is observed (Fig. 8), which is attributed to adsorbed ethanol residues blocking the active sites of the catalysts [22,44]. Since the initial slopes on the curves for both catalysts are similar, it seems that their poisoning rates are comparable. During the rest of time more active Pd-Ni/C loses its activity faster than Pd/C. This is consistent with the potentiodynamic stability test (Fig. 6a), in which Pd-Ni/C exhibits a higher initial activity as well, but also a higher activity loss. At the end of the test the current density on Pd-Ni/C was higher than on Pd/C by a factor of 1.5.

The potential of 0.7 V corresponds to the beginning of the formation of Pd(II)-oxide, according to the voltammograms in Fig. 4. Since the deactivation of Pd in Pd/C at this constant potential is not negligible as in the potentiodynamic test, this could mean that the

Table 1
Electrochemically active surface area of Pd and mass activities for the EOR of the Pd-Ni/C and Pd/C catalysts determined under the potentiodynamic conditions (as a function of the cycle number) and under the potentiostatic conditions (as a function of time).

		Potentiodynamic test at 50 mV s^{-1}								Potentiostatic test at 0.7 V	
	EASA/m^2 g^{-1}	j_{max}/mA mg^{-1}				$j_{0.7V}$/mA mg^{-1}				j/mA mg^{-1}	
		2nd	5th	50th	250th	2nd	5th	50th	250th	1 min	25 min
Pd-Ni/C	75.8	1575	1722	2010	1158	924	1010	1158	749	563	256
Pd/C	57.4	623	617	684	556	454	480	559	466	223	129

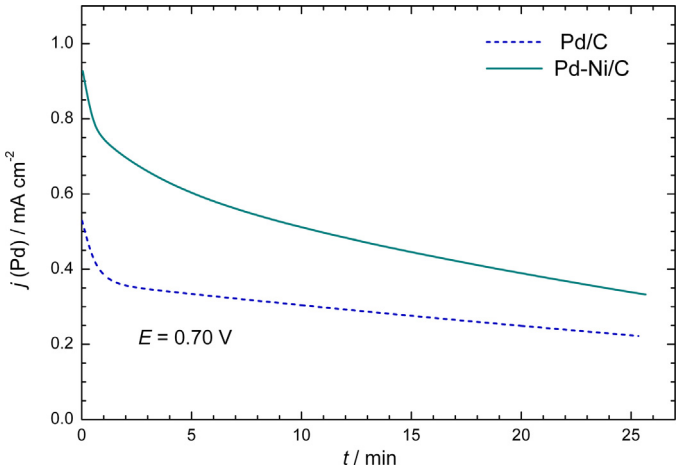

Fig. 8. Potentiostatic curves for the EOR on Pd/C and Pd-Ni/C recorded at 0.7 V in 0.1 M NaOH containing 0.5 M C_2H_5OH.

coverage by Pd(II)-oxide gradually increases if the oxide is not periodically removed by electrochemical reduction. It should be noted that Pd is very stable in alkaline media [45], thus the dissolution of Pd as a possible reason of deactivation of Pd/C is not to be expected.

The current normalized to the surface area of the electroactive metal (current density or specific activity, SA) describes the intrinsic activity of a catalyst, but the current normalized to the mass of the electroactive metal (mass activity, MA) is important for its practical application. The results of potentiodynamic (Fig. 6) and potentiostatic (Fig. 8) examination of the EOR on Pd/C or Pd-Ni/C, expressed as SA and MA, are summarized in Table 1. The average values of the EASA of Pd determined from more than ten independent measurements, which are used for the calculation of mass activity, are also given in Table 1.

The evaluation of the performance of Pd-Ni/C and Pd/C based on their SA values revealed that the presence of Ni in the catalyst increases the activity of Pd under both potentiodynamic and potentiostatic conditions. When the MA values of the two catalysts are compared, the effect of Ni is even larger, which is the consequence of higher EASA of Pd in Pd-Ni/C than in Pd/C catalyst. In other words, Ni improved dispersion of Pd on the carbon support as well as its intrinsic activity for the EOR.

Although straightforward comparison of data from studies of different research groups is difficult because of different experimental conditions and because the currents are usually only reported per geometric area of the electrode, we have tried to contrast our results with several recently published works focused on Pd-Ni catalysts. Ahmed and Jeon [22] reported a maximum current of the forward potentiodynamic curve of 615 A g^{-1} for their most active $Pd_{50}Ni_{50}$ binary alloyed catalyst, which is lower than the values in our work. Zhang et al. [18] reported SA of 3.3 mA cm^{-2} and 3.5 mA cm^{-2} for the unalloyed and alloyed PdNi nanoparticles, respectively, determined at maximum of potentiodynamic curves in 1 M NaOH containing 1 M ethanol. This is close to our 2.7 mA cm^{-2} measured in 0.1 M NaOH containing 0.5 M ethanol. The MA values are also similar, between 1938 A g^{-1} and 2368 A g^{-1} in the work of Zhang et al. [18] and 2010 A g^{-1} in our measurements. Another research group [20] found that a core-shell structured Ni-Pd catalyst possessed 2.3 higher MA than pure Pd nanocatalyst if their maximums at potentiodynamic curves are considered. In our experiments this ratio is between 2 and 3, depending on the cycle number. The maximum MA of about 2000 A g^{-1} in our study is lower than 3500 A g^{-1} reported in the work of Zhang et al. [20], but their measurements were done in the electrolyte with a higher pH and ethanol concentration, which increased the EOR rate.

In a systematic review of Brouzgou et al. [46], the maximum current density of EOR versus Pd loading on the electrode were plotted for various Pd-containing catalysts for application in DEFC with anion exchange membrane. Most of the data lay between 15 mA μg^{-1}_{Pd} and 0.25 mA μg^{-1}_{Pd}. The best performance, even over 15 mA μg^{-1}_{Pd}, exhibited Pd nanoparticles dispersed in 3,4-polyethylenedioxythiophene [47] and a composite of AuPd–WC/C [48], while at the lower limit is the activity of nanoporous Pd composites prepared by de-alloying of Al_3Pd intermetallic compound [49]. The catalyst with an activity similar to 2 mA μg^{-1}_{Pd} reached on Pd-Ni/C catalyst in this work is alloyed Pd_3Au/C [50].

4. Conclusions

Pd/C and Pd-Ni/C catalysts were synthesized employing a borohydride reduction method. XRD showed pure Pd particles of 3 ± 1 nm in diameter in Pd/C, while in Pd-Ni/C apart from Pd, PdO and Ni were also detected. The Pd crystallite size in this catalyst was 2 ± 1 nm. TEM characterization of Pd/C indicated mean diameter of 3.7 nm. In Pd-Ni/C sample certain agglomeration of Pd particles were observed. The mean diameter of Pd particles was estimated to be 3.3 nm. EDX elemental mapping showed that Ni is distributed relatively evenly across the carbon support, while palladium forms discrete particles on it. Such a structure of the catalyst is different from the other Pd-Ni catalysts reported in literature.

Cyclic voltammetry of Pd-Ni/C confirmed the presence of Ni on the catalyst surface. EASA of Pd was estimated from the charge under the Pd(II)-oxide reduction peak for both Pd/C and Pd-Ni/C catalysts and used for determining specific and mass activity for the EOR.

The activity of the Pd-Ni/C and Pd/C catalysts for the EOR was tested under the potentiodynamic and potentiostatic conditions. Both types of experiments showed that Pd-Ni/C is more active for the EOR, either expressed as SA or MA. During the potentiodynamic stability test an interesting phenomenon of activation of the Pd-Ni/C catalyst was observed. It was found that maximum activity is attained after fifty cycles with a positive potential limit of 1.2 V, regardless of whether they were performed in the electrolyte with or without ethanol. It was postulated that potential cycling of the Pd-Ni surface causes reorganization of the catalyst surface bringing Pd and Ni sites to a more suitable arrangement for the efficient ethanol oxidation.

The present study confirms that Pd-Ni bi-metal nanoparticles are prospective anode electrocatalysts in DEFC and that an impor-

tant point in the catalyst design is the suitable arrangement of Pd and Ni sites.

Acknowledgements

This work was financially supported by the Ministry of Education, Science and Technological Development of the Republic of Serbia, Contract No. ON-172054. VRR acknowledges support by Serbian Academy of Sciences and Arts under contract #F-141.

Appendix A. Supplementary data

Supplementary data associated with this article can be found, in the online version, at http://dx.doi.org/10.1016/j.apcatb.2016.02.039.

References

[1] E. Antolini, Catalysts for direct ethanol fuel cells, J. Power Sources 170 (2007) 1–12.
[2] A. Rabis, P. Rodriguez, T.J. Schmidt, Electrocatalysis for polymer electrolyte fuel cells: recent achievements and future challenges, ACS Catal. 2 (2012) 864–890.
[3] B. Hahn-Hägerdal, M. Galbe, M.F. Gorwa-Grauslund, G. Lidén, G. Zacchi, Bio-ethanol – the fuel of tomorrow from the residues of today, Trends Biotechnol. 24 (2006) 549–556.
[4] S. Song, W. Zhou, Z. Liang, R. Cai, G. Sun, Q. Xin, V. Stergiopoulos, P. Tsiakaras, The effect of methanol and ethanol cross-over on the performance of PtRu/C-Based anode DAFCS, Appl. Catal. B: Environ. 55 (2005) 65–72.
[5] L. Jiang, A. Hsu, D. Chu, R. Chen, Ethanol electro-oxidation on Pt/C and PtSn/C catalysts in alkaline and acid solutions, Int. J. Hydrogen Energy 35 (2010) 365–372.
[6] L. Ma, D. Chu, R. Chen, Comparison of ethanol electro-oxidation on Pt/C and Pd/C catalysts in alkaline media, Int. J. Hydrogen Energy 37 (2012) 11185–11194.
[7] C. Xu, L. Cheng, P. Shen, Y. Liu, Methanol and ethanol electrooxidation on Pt and Pd supported on carbon microspheres in alkaline media, Electrochem. Comm. 9 (2007) 997–1001.
[8] C. Xua, P.K. Shen, Y. Liu, Ethanol electrooxidation on Pt/C and Pd/C catalysts promoted with oxide, J. Power Sources 164 (2007) 527–531.
[9] C. Bianchini, P.K. Shen, Palladium-Based electrocatalysts for alcohol oxidation in half cells and in direct alcohol fuel cells, Chem. Rev. 109 (2009) 4183–4206.
[10] E. Antolini, J. Perez, Anode catalysts for alkaline direct alcohol fuel cells and characteristics of the catalyst layer, in: M. Shao (Ed.), Electrocatalysis in Fuel Cells, Springer-Verlag, London, 2013.
[11] (accessed 28.8.2015) http://www.platinum.matthey.com/.
[12] J.R. Varcoe, R.C.T. Slade, E.L.H. Yee, An alkaline polymer electrochemical interface: a breakthrough in application of alkaline anion-exchange membranes in fuel cells, Chem. Comm. 13 (2006) 1428–1429.
[13] P.K. Shen, C. Xu, Alcohol oxidation on nanocrystalline oxide Pd/C promoted electrocatalysts, Electrochem. Comm. 8 (2006) 184–188.
[14] T.G. Nikiforova, O.A. Datskevich, V.V. Maleev, Palladium catalysts on porous nickel substrates for alcohol fuel cells, Russ. J. Appl. Chem. 85 (2012) 1871–1878.
[15] F. Hu, C. Chen, Z. Wang, G. Wei, P.K. Shen, Mechanistic study of ethanol oxidation on Pd–NiO/C electrocatalyst, Electrochim. Acta 52 (2006) 1087–1091.
[16] Y.-L. Wang, Y.-Q. Zhao, C.-L. Xu, D.-D. Zhao, M.-W. Xu, Z.-X. Su, H.-L. Li, Improved performance of Pd electrocatalyst supported on three-dimensional nickel foam for direct ethanol fuel cells, J. Power Sources 195 (2010) 6496–6499.
[17] S.Y. Shen, T.S. Zhao, J.B. Xu, Y.S. Li, Synthesis of PdNi catalysts for the oxidation of ethanol in alkaline direct ethanol fuel cells, J. Power Sources 195 (2010) 1001–1006.
[18] Z. Zhang, L. Xin, K. Sun, W. Li, Pd–Ni electrocatalysts for efficient ethanol oxidation reaction in alkaline electrolyte, Int. J. Hydrogen Energy 36 (2011) 11686–11697.
[19] Z. Qi, H. Geng, X. Wang, C. Zhao, H. Ji, C. Zhang, J. Xu, Z. Zhang, Novel nanocrystalline PdNi alloy catalyst for methanol and ethanol electro-oxidation in alkaline media, J. Power Sources 196 (2011) 5823–5828.
[20] M. Zhang, Z. Yan, J. Xie, Core/shell Ni@Pd nanoparticles supported on MWCNTs at improved electrocatalytic performance for alcohol oxidation in alkaline media, Electrochim. Acta 77 (2012) 237–243.
[21] C.-H.A. Tsang, K.N. Hui, K.S. Hui, L. Rend, Deposition of Pd/graphene aerogel on nickel foam as a binder-free electrode for direct electrooxidation of methanol and ethanol, J. Mat. Chem. A 2 (2014) 17986–17993.
[22] M.S. Ahmed, S. Jeon, Highly active graphene-Supported Ni_xPd_{100-x} binary alloyed catalysts for electro-Oxidation of ethanol in an alkaline media, ACS Catal. 4 (2014) 1830–1837.
[23] J.A.D. del Rosario, J.D. Ocon, H. Jeon, Y. Yi, J.K. Lee, J. Lee, Enhancing role of nickel in the nickel-Palladium bilayer for electrocatalytic oxidation of ethanol in alkaline media, J. Phys. Chem. C 118 (2014) 22473–22478.
[24] A. Dutta, J. Datta, Energy efficient role of Ni/NiO in PdNi nano catalyst used in alkaline DEFC, J. Mat. Chem. A 2 (2014) 3237–3250.
[25] X. Fang, L. Wang, P.K. Shen, G. Cui, C. Bianchini, An in situ Fourier transform infrared spectroelectrochemical study on ethanol electrooxidation on Pd in alkaline solution, J. Power Sources 195 (2010) 1375–1378.
[26] Z.-Y. Zhou, Q. Wang, J.-L. Lin, N. Tian, S.-G. Sun, In situ FTIR spectroscopic studies of electrooxidation of ethanol on Pd electrode in alkaline media, Electrochim. Acta 55 (2010) 7995–7999.
[27] Z.X. Liang, T.S. Zhao, J.B. Xu, L.D. Zhu, Mechanism study of the ethanol oxidation reaction on palladium in alkaline media, Electrochim. Acta 54 (2009) 2203–2208.
[28] G. Cui, S. Song, P.K. Shen, A. Kowal, C. Bianchini, First-principles considerations on catalytic activity of Pd toward ethanol oxidation, J. Physic. Chem. C 113 (2009) 15639–15642.
[29] L. Wang, A. Lavacchi, M. Bellini, F. D'Acapito, F. Di Benedetto, M. Innocenti, H.A. Miller, G. Montegrossi, C. Zafferoni, F. Vizza, Deactivation of palladium electrocatalysts for alcohols oxidation in basic electrolytes, Electrochim. Acta (2015), http://dx.doi.org/10.1016/j.electacta.2015.02.026 (Available online 16 February 2015, ISSN 0013-4686).
[30] K.A. Kuttiyiel, K. Sasaki, D. Su, M.B. Vukmirovic, N.S. Marinkovic, R.R. Adzic, Pt monolayer on Au-stabilized PdNi core–shell nanoparticles for oxygen reduction reaction, Electrochim. Acta 110 (2013) 267–272.
[31] M. Liao, Q. Hu, J. Zheng, Y. Li, H. Zhou, C.-J. Zhong, B.H. Chen, Pd decorated Fe/C nanocatalyst for formic acid electrooxidation, Electrochim. Acta 111 (2013) 504–509.
[32] TOPAS V.21: General Profile and Structure Analysis Software for Powder Diffraction Data, User Manual, Bruker AXS: Karlsruhe, Germany, 2003.
[33] B.D. Cullity, Elements of X-Ray Diffraction, Addison-Wesley Publishing Company, Boston, 1978, pp. 102.
[34] M. Grdén, K. Klimek, A. Czerwiński, A quartz crystal microbalance study on a metallic nickel electrode, J. Solid State Electrochem. 8 (2004) 390–397.
[35] S.A.S. Machado, L.A. Avaca, The hydrogen evolution reaction on nickel surfaces stabilized by H-absorption, Electrochim. Acta 39 (1994) 1385–1391.
[36] M.D. Obradović, S.Lj. Gojković, Pd black decorated by Pt sub-monolayers as an electrocatalyst for the HCOOH oxidation, J. Solid State Electrochem. 18 (2014) 2599–2607.
[37] A.E. Bolzán, Phenomenological aspects related to the electrochemical behaviour of smooth palladium electrodes in alkaline solutions, J. Electroanal. Chem. 380 (1995) 127–138.
[38] M. Grdeń, Electrochemical quartz crystal microbalance studies of a palladium electrode oxidation in a basic electrolyte solution, Electrochim. Acta 54 (2009) 909–920.
[39] A. Czerwiński, The adsorption of carbon oxides on a palladium electrode from acidic solution, J. Electroanal. Chem. 379 (1994) 487–493.
[40] D.A.J. Rand, R.J. Woods, The nature of adsorbed oxygen on rhodium, palladium and gold electrodes, J. Electroanal. Chem. 31 (1971) 29–38.
[41] M. Wang, W. Zhang, J. Wang, D. Wexler, S.D. Poynton, R.C.T. Slade, H. Liu, B. Winther-Jensen, R. Kerr, D. Shi, J. Chen, PdNi hollow nanoparticles for improved electrocatalytic oxygen reduction in alkaline environments, ACS Appl. Mater. Inter. 5 (2013) 12708–12715.
[42] M. Watanabe, S. Motoo, Electrocatalysis by ad-atoms: part II. Enhancement of the oxidation of methanol on platinum by ruthenium ad-atoms, J. Electroanal. Chem. 60 (1975) 267–273.
[43] M. Grdeń, A. Czerwiński, EQCM studies on Pd–Ni alloy oxidation in basic solution, J. Solid State Electrochem. 12 (2008) 375–385.
[44] E.A. Monyoncho, S. Ntais, F. Soares, T.K. Woo, E.A. Baranova, Synergetic effect of palladium-ruthenium nanostructures for ethanol electrooxidation in alkaline media, J. Power Sources 287 (2015) 139–149.
[45] M. Grdén, J. Kotowski, A. Czerwiński, The study of electrochemical palladium behavior using the quartz crystal microbalance, J. Solid State Electrochem. 4 (2000) 273–278.
[46] A. Brouzgou, A. Podias, P. Tsiakaras, PEMFCs and AEMFCs directly fed with ethanol: a current status comparative review, J. Appl. Electrochem. 43 (2013) 119–136.
[47] R.K. Pandey, V. Lakshminarayanan, Enhanced electrocatalytic activity of Pd-Dispersed 3,4-Polyethylenedioxythiophene Film in hydrogen evolution and ethanol electro-oxidation reactions, J. Phys. Chem. C 114 (2010) 8507–8514.
[48] M. Nie, H. Tang, Z. Wei, S.P. Jiang, P.K. Shen, Highly efficient AuPd–WC/C electrocatalyst for ethanol oxidation, Electrochem. Commun. 9 (2007) 2375–2379.
X. Wang, W. Wang, Z. Qi, C. Zhao, H. Ji, Z. Zhang, Fabrication, microstructure and electrocatalytic property of novel nanoporous palladium composites, J. Alloy Compd. 508 (2010) 463–470.
[50] J.B. Xu, T.S. Zhao, S.Y. Shen, Y.S. Li, Stabilization of the palladium electrocatalyst with alloyed gold for ethanol oxidation, Int. J. Hydrogen Energy 35 (2010) 6490–6500.